ZAMM · Z. Angew. Math. Mech. **87**, No. 7, 486 – 498 (2007) / **DOI** 10.1002/zamm.200610331

Interactive boundary layer in a Hele Shaw cell

Pierre-Yves Lagrée*

Laboratoire de Modélisation en Mécanique, UMR CNRS 7607, Université Pierre et Marie Curie, Boîte 162, 4 place Jussieu, 75252 Paris, France

Received 30 June 2006, accepted 8 May 2007
Published online 25 July 2007

Key words asymptotic methods, Interactive Boundary Layer, Hele Shaw cell

The steady laminar flow in a rectangular Hele Shaw cell is considered at high Reynolds number. The lower thin wall layer is perturbed by a small bump. Averaged equations obtained in averaging the Navier Stokes equations across the thin direction are used. This procedure allows to recover the nonlinear convective term in the equations. First a classical Boundary Layer theory is constructed, the weak coupling leads to a singularity. An Interacting Boundary Layer theory is then constructed in order to compute the strong coupling of the "Averaged ideal fluid" and the "Averaged boundary layer". The "triple deck" counter part is presented as well. An asymptotic nonlinear approximation of the flow can be computed with short computation time. Positive comparisons of computation of the full Averaged Navier Stokes equation and Interacting Boundary Layer theory are shown. For instance, the boundary layer separation over a bump is obtained when either the bump height or the Reynolds number is increased.

1 Introduction

The Hele cell is known for its analogy with ideal fluids. It is used as an experimental setup for various experiments. When used in the classical way (Batchelor [1]), only pressure gradients and viscous forces are present in the flow description. But some experiments can only be explained if the nonlinear convective terms are reintroduced. For example Gondret and Rabaud [8], Gondret et al. [9] reintroduced the convective terms to model a Kelvin-Helmholtz instability (see also Plouraboué et al. [19], Hinch and Plouraboué [12]). The basic flow is computed in Gondret et al. [10], showing the boundary layers at the walls. The key point is to inject, thanks to some strong approximation, the nonlinear convective derivative term in the equations. This approximation assumes that the transverse shape of the velocity is always a Poiseuille shape. Thus, Gondret et al. used a simplified bidimensional equation obtained by integrating the three-dimensional Navier-Stokes equations across the width of the cell. They obtained good agreement between experiments and theory for a Kelvin-Helmholtz instability. Because the process of averaging is crude, the equations were revisited by Ruyer-Quil [21] who presented an improved averaging. His overall system is the same, but his coefficients are slightly different.

Here, we take those equations as granted and will not discuss them. Having in mind the flow over a bumpy wall (in fact thin ripples or thin dunes, Loiseleux et al. [16]) we wish to compute how the flow is pertubed by this indentation and to evaluate the skin friction on this wall (or at least the mean value of it over the width of the cell). A direct numerical resolution can be time consuming, because there are lot of scales of various small or large ratio in this problem (e.g. the ratio of the width to length of the cell is small). Therefore we use asymptotic expansions to solve the flow. We decompose it in layers: an ideal fluid layer, and a viscous boundary layer.

Starting from this special system (Sect. 2), we develop the standard method of Boundary Layer theory following the classical textbooks (Schlichting [22]). First we compute the external velocity from the "Averaged Euler Equations" (Sect. 2.2), next we settle the associated boundary layer equations (Sect. 2.3). We then present the "standard problem" or "direct problem" of boundary layer (Sect. 3.1). We compute some examples and show that we can compute the flow up to the point of vanishing shear. With this method boundary layer separation is singular. So we present next the Interacting Boundary Layer theory for this special flow (Sect. 3.3). This theory allows boundary layer separation (we present as well a Triple Deck description, Sect. 3.2). We compare in Sect. 4 the full Averaged Navier Stokes numerical resolution to the Averaged Interacting Boundary Layer (IBL). In the Appendix we present a simplified von Kármán resolution and some explanations on the resolution of the inverse boundary layer equations with strong coupling.

* e-mail: pyl@ccr.jussieu.fr, www.lmm.jussieu.fr/~lagree

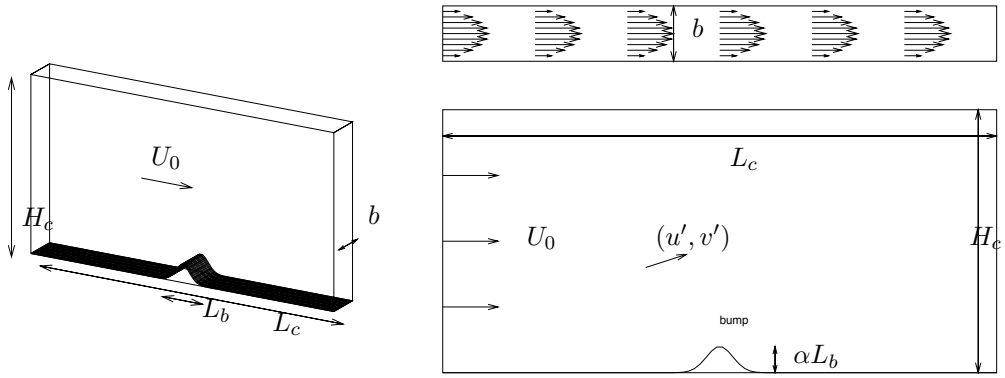

Fig. 1 Left: the 3D Hele Shaw cell, of size L_c, H_c, b ($b \ll L_c$ and $b \ll H_c$). The bump is of length L_b. The relative height of the bump is $\alpha \ll 1$. Right top: the transverse profiles are supposed Poiseuille ones. Right bottom: the equivalent 2D domain where the averaged systems have to be solved. The lower boundary is pertubed by the small bump.

2 Averaged equations

2.1 Averaged Navier Stokes equations

We consider a steady incompressible viscous flow in a Hele Shaw cell which satisfies the Navier Stokes equations. The cell is of very small width b. All the walls are flat, except the lower one where there is a small bump, see Fig. 1. This bump is of height smaller than its length (of order $\alpha \ll 1$ say), and of width b (in the z direction). The position of the bump is the reference point of the co-ordinates. The entrance is at the left, the exit at the right. The mainstream direction is x, the vertical direction is y. The order of magnitude of the fluid flow velocity is U_0. For a thin Hele Shaw cell, it is classical to consider that the z dependance of the velocity is of Poiseuille type. So, supposing that the velocity profiles remain of parabolic shape in z (Fig. 1 right top), we define the prime velocities $u(x,y,z) = \frac{3}{2}(1-(\frac{z}{b/2})^2)u'(x,y)$, $w = 0$, and $v(x,y,z) = \frac{3}{2}(1-(\frac{z}{b/2})^2)v'(x,y)$, and the prime pressure: $p(x,y,z) = p'(x,y)$.

The method developed by Gondret et al. [8,9] is to integrate the three-dimensional equations along z, and to assume that the velocity in this direction can be neglected: $w = 0$. Gravity effects are neglected too, but may be introduced. With the chosen Poiseuille velocity profiles, the integrated system of incompressibility and of momentum balance is twodimensional:

$$\left(\frac{\partial u'}{\partial x} + \frac{\partial v'}{\partial y}\right) = 0\,, \tag{1}$$

$$\gamma_2\left(u'\frac{\partial}{\partial x} + v'\frac{\partial}{\partial y}\right)u' = -\frac{\partial}{\rho\partial x}p' + \nu\gamma_1\left(\frac{\partial^2}{\partial x^2} + \frac{\partial^2}{\partial y^2}\right)u' - \frac{12\nu}{b^2}u'\,, \tag{2}$$

$$\gamma_2\left(u'\frac{\partial}{\partial x} + v'\frac{\partial}{\partial y}\right)v' = -\frac{\partial}{\rho\partial y}p' + \nu\gamma_1\left(\frac{\partial^2}{\partial x^2} + \frac{\partial^2}{\partial y^2}\right)v' - \frac{12\nu}{b^2}v'\,, \tag{3}$$

with $\gamma_2 = \frac{6}{5}$ and $\gamma_1 = 1$. These coefficients come from the transverse integration. Ruyer-Quil [21] developed the method of "weightened residual" which gives a better approximation of these coefficients: $\gamma_2 = \frac{54}{35}$ and $\gamma_1 = \frac{6}{5}$. The additional term to classical 2D Navier Stokes equations is the Darcy one. We obtain Brinkman equations with the nonlinear term.

Writing $x = \gamma_2 L\bar{x}$, $y = \gamma_2 L\bar{y}$ (same spatial scales), $u' = U_0\bar{u}$, $v' = U_0\bar{v}$, $p' = \gamma_2\rho U_0^2\bar{p}$ (same velocity scales), and choosing $L = \frac{b}{12}\left(\frac{U_0 b}{\nu}\right)$ (by a van Dyke [27], Darrozès [5] "least degeneracy" principle) we write the non-dimensional final system as:

$$\left(\frac{\partial\bar{u}}{\partial\bar{x}} + \frac{\partial\bar{v}}{\partial\bar{y}}\right) = 0, \tag{4}$$

$$\left(\bar{u}\frac{\partial\bar{u}}{\partial\bar{x}} + \bar{v}\frac{\partial\bar{u}}{\partial\bar{y}}\right) = -\frac{\partial\bar{p}}{\partial\bar{x}} - \bar{u} + \frac{1}{\mathrm{Re}}\left(\frac{\partial^2\bar{u}}{\partial\bar{x}^2} + \frac{\partial^2\bar{u}}{\partial\bar{y}^2}\right), \tag{5}$$

$$\left(\bar{u}\frac{\partial\bar{v}}{\partial\bar{x}} + \bar{v}\frac{\partial\bar{v}}{\partial\bar{y}}\right) = -\frac{\partial\bar{p}}{\partial\bar{y}} - \bar{v} + \frac{1}{\mathrm{Re}}\left(\frac{\partial^2\bar{v}}{\partial\bar{x}^2} + \frac{\partial^2\bar{v}}{\partial\bar{y}^2}\right), \tag{6}$$

where we have defined a gap Reynolds number $R_b = \left(\frac{U_0 b}{\nu}\right)$ and a "L" based Reynolds $\mathrm{Re} = \left(\frac{U_0 L \gamma_2^2}{\gamma_1 \nu}\right)$. We note the following relation between the two Reynolds numbers: $\mathrm{Re} = \frac{R_b^2 \gamma_2^2}{12\gamma_1}$, and that γ_1 and γ_2 have disappeared from the equations.

This L corresponds to the entry length of the cell. It is analogous to the problem of entry in a pipe (Schlichting [22]). Hence, the entrance effect is located at the left of the cell on scale L. The bump is located at a distance larger than L. In order to be self consistent, the order of magnitude of the length bump is L.

In experiments from Gondret et al. [10] or Loiseleux [16] the values are: $b = 0.002\,\mathrm{m}$, as $500 < (R_b = \frac{U_0 b}{\nu}) < 1200$, we have $8\,\mathrm{cm} < L < 20\,\mathrm{cm}$ and $0.002 < \mathrm{Re}^{-1/2} < 0.006$ (or $3 \cdot 10^4 < \mathrm{Re} < 1.7 \cdot 10^5$).

Finally, the boundary condition is the no slip condition at the lower and upper boundaries (see Fig. 1 right bottom). A pressure drop between the entrance and the output is imposed to drive the flow; alternatively the first velocity profile is given at entrance and the pressure is set to 0 at output.

2.2 Averaged Euler equations

We now use an asymptotic expansion to deal with this system in a classical ideal fluid/boundary layer framework. We show that with this approach we cannot compute boundary layer separation. If Re is large, then the second order derivatives disappear, and from (5), (6), and (4) we have the "Averaged Euler" system (Gondret and Rabaud [8]):

$$\left(\frac{\partial \bar{u}}{\partial \bar{x}} + \frac{\partial \bar{v}}{\partial \bar{y}}\right) = 0\,, \tag{7}$$

$$\left(\bar{u}\frac{\partial \bar{u}}{\partial \bar{x}} + \bar{v}\frac{\partial \bar{u}}{\partial \bar{y}}\right) = -\frac{\partial \bar{p}}{\partial \bar{x}} - \bar{u}\,, \tag{8}$$

$$\left(\bar{u}\frac{\partial \bar{v}}{\partial \bar{x}} + \bar{v}\frac{\partial \bar{v}}{\partial \bar{y}}\right) = -\frac{\partial \bar{p}}{\partial \bar{y}} - \bar{v}\,. \tag{9}$$

These are Darcy equations with nonlinear convection. The boundary condition is now the slip condition at the lower and upper boundary for the velocity. So $\bar{u} = 1$, $\bar{v} = 0$, and $\bar{p} = -\bar{x}$ is the basic solution of (8), (9), and (7) in a rectangular cell.

We introduce a small bump of length L_b and of height αL_b. For consistency the scale of the bump is $L_b = L$. As the bump is small (with $\alpha \ll 1$), we seek a linearized solution (small perturbation theory and transfer of boundary conditions van Dyke [27]): $\bar{u} = 1 + \alpha\bar{u}_1 + \ldots$, $\bar{v} = \alpha\bar{v}_1 + \ldots$, and $\bar{p} = -\bar{x} + \alpha\bar{p}_1 + \ldots$. We linearize the slip condition at the lower boundary as:

$$\frac{\bar{v}}{\bar{u}} = \alpha\frac{d\bar{f}}{d\bar{x}} \quad i.e. \alpha\bar{v}_1(\bar{x}, 0) + O(\alpha^2) = \alpha\frac{d\bar{f}}{d\bar{x}}\,. \tag{10}$$

Hence, the system (8), (9), and (7) now reads :

$$\frac{\partial^2 \bar{p}_1}{\partial \bar{x}^2} + \frac{\partial^2 \bar{p}_1}{\partial \bar{y}^2} = 0, \qquad \frac{\partial \bar{p}_1(\bar{x}, 0)}{\partial \bar{y}} = -\frac{d\bar{f}(\bar{x})}{d\bar{x}} - \frac{d^2\bar{f}(\bar{x})}{d\bar{x}^2}\,. \tag{11}$$

We solve (11) with no perturbation far from the lower boundary (the cell is high enough) in Fourier space. This gives the values of pressure and velocity perturbations at the boundary itself as:

$$FT[\bar{p}_1] = -(1 + (-ik))\frac{ik}{|k|}FT[\bar{f}]\,, \qquad FT[\bar{u}_1] = |k|FT[\bar{f}]\,. \tag{12}$$

Coming back in physical space (here fp denotes the finite part of the integral):

$$\bar{u}_1 = \frac{1}{\pi} fp \int_{-\infty}^{\infty} \frac{d\bar{f}/d\bar{x}}{\bar{x} - \xi} d\xi\,. \tag{13}$$

A given perturbation of the boundary gives the slip velocity $\bar{U}_e = 1 + \alpha\bar{u}_1 + O(\alpha^2)$. This is exactly the same formula as for classical 2D ideal fluid, but the perturbation of pressure will be different. We have to introduce a boundary layer in order to recover the no slip condition at the boundary.

2.3 Averaged boundary layer

2.3.1 Averaged boundary layer equations

Writing the non dimensional Eqs. (5), (6), and (4) with again $\bar{x} = \tilde{x}$, $\bar{u} = \tilde{u}$, $\bar{p} = \tilde{p}$, but now focusing at a very small scale in the transverse direction: $\bar{y} = (\delta/(\gamma_2 L))\tilde{y}$ and $\bar{v} = (\delta/(\gamma_2 L))\tilde{v}$, with $(\delta/L) \ll 1$. We choose $\delta/(\gamma_2 L) = \mathrm{Re}^{-1/2}$, to keep the transverse derivative term and this gives $\delta = b/(\sqrt{12/\gamma_1})$. This is again the van Dyke [27], Darrozès [5] principle, and also the classical boundary layer point of view (Schlichting [22], Gersten and Herwig [7]). The boundary layer scale is the scale of the distance between the plates (b). The Averaged Boundary Layer equations read:

$$\left(\frac{\partial \tilde{u}}{\partial \bar{x}} + \frac{\partial \tilde{v}}{\partial \tilde{y}}\right) = 0\,, \tag{14}$$

$$\left(\tilde{u}\frac{\partial \tilde{u}}{\partial \bar{x}} + \tilde{v}\frac{\partial \tilde{u}}{\partial \tilde{y}}\right) = -\frac{\partial \tilde{p}}{\partial \bar{x}} + \frac{\partial^2 \tilde{u}}{\partial \tilde{y}^2} - \tilde{u}\,, \tag{15}$$

$$0 = -\frac{\partial \tilde{p}}{\partial \tilde{y}}\,. \tag{16}$$

The relative boundary layer thickness δ/L should be smaller than the relative size of the bump α in classical boundary layer theory. In fact $\tilde{y}$ is taken from the boundary itself in the normal direction. Nevertheless, we will see in the next section that δ/L and α may be of the same amplitude, so by anticipation $\tilde{f} = \bar{f}$. We may do a Prandtl transform ($\bar{x} \to \bar{x}$, $\tilde{y} \to \tilde{y} - \tilde{f}(\bar{x})$, and $\tilde{v} \to \tilde{v} - \frac{d\tilde{f}}{d\bar{x}}\frac{\partial \tilde{u}}{\partial \bar{x}}$), so that the transformed boundary is flat with this new variables.

The boundary conditions are first the no slip condition at the lower boundary $\tilde{u}(\bar{x}, 0) = 0$, $\tilde{v}(\bar{x}, 0) = 0$: the effort has been done to reobtain this. The matching condition $\tilde{u}(\bar{x}, \tilde{y} \to \infty) = \bar{u}(\bar{x}, \bar{y} \to 0)$ gives $\tilde{u}(\bar{x}, \infty) = \bar{U}_e(\bar{x})$ and there is no matching to be done with the transverse velocity at this order. We note that $\tilde{p}$ is function of $\bar{x}$ only and matches with the ideal fluid pressure $\bar{p}(\bar{x}, 0)$, and the pressure may be removed from the equation: $\bar{U}_e\frac{d\bar{U}_e}{d\bar{x}} + \bar{U}_e = -\frac{d\bar{p}}{d\bar{x}}$ (recall $\bar{x} = \bar{x}$, and see Appendix I).

The two main results of the computation are $\tilde{\delta}_1 = \int_0^\infty (1 - \frac{\tilde{u}}{\bar{U}_e})d\tilde{y}$ the boundary layer displacement thickness and $\tilde{\tau} = \frac{\partial \tilde{u}}{\partial \tilde{y}}(\bar{x}, 0)$ the (mean) shear (or skin friction) at the lower wall. The boundary layer displacement δ_1 once rescaled by $\mathrm{Re}^{-1/2}$ represents for the ideal fluid a perturbation at order $\mathrm{Re}^{-1/2}$. This ideal fluid perturbation may be solved, leading to a boundary layer problem at order two. And so on. This leads to a cascade of developments at successively increasing orders (van Dyke [27]). This is called weak interaction.

2.3.2 Basic averaged boundary layer

The basic boundary layer flow consists in solving (14) and (15) with $\tilde{u}(\bar{x}, 0) = 0$, $\tilde{v}(\bar{x}, 0) = 0$, and $\tilde{u}(\bar{x}, \infty) = 1$. The ideal flow is $\bar{u} = 1$ and $\bar{p} = -\bar{x}$, so that the solution of

$$0 = -\frac{\partial p}{\partial \bar{x}} + \frac{\partial^2 \tilde{u}}{\partial \tilde{y}^2} - \tilde{u} \quad \text{is} \quad \tilde{u}_B = 1 - e^{-\tilde{y}}\,. \tag{17}$$

The basic Boundary Layer thickness is $\tilde{\delta}_{1B} = 1$ and the basic skin friction is $\tilde{\tau}_B = 1$. The scaled mean shear stress at the wall is then $\frac{\partial u}{\partial y} = \frac{\sqrt{12/\gamma_1}}{b}U_0$, with $\sqrt{12/\gamma_1} = 3.46$ or 3.16 if $\gamma_1 = 1$ or $6/5$. Note that the exact value (which is 3.26) has been computed by Loiseleux et al [16]. This problem of Basic Averaged Boundary Layer (Eq. (17)) is obtained from the average of the full Navier Stokes equation (here scaled with b):

$$0 = 1 + \left(\frac{\partial^2}{\partial \hat{z}^2} + \frac{\partial^2}{\partial \hat{y}^2}\right)\hat{u}, \tag{18}$$

with no slip boundary conditions $\hat{u}(\hat{y}, \hat{z} = \pm 1/2) = 0$, $\hat{u}(\hat{y} = 0, \hat{z}) = 0$, and $\partial \hat{u}(\hat{y}, \hat{z})/\partial \hat{y} = 0$ for $\hat{y} \gg 1$. The solutions of problem (Eq. (18)) is computed with the free software FreeFem++ [11], the solution is plotted on Fig. 2. The solution of the problem 17 (note that $\tilde{y} = \sqrt{12/\gamma_1}\hat{y}$) is plotted on same figure. The agreement is very good for $\gamma_1 = 1$, if we take $\gamma_1 = 6/5$, solutions of the two problems are superposed.

3 Final fluid problem

3.1 Classical "direct" boundary layer resolution

Having the topography $\alpha\bar{f}$, we compute the velocity perturbation using (13) and then the boundary layer. Taking $\alpha \to 0$, the slip velocity is simply $\bar{U}_e = 1$, and the problem in the boundary layer is solved by the exponential profile. So the full

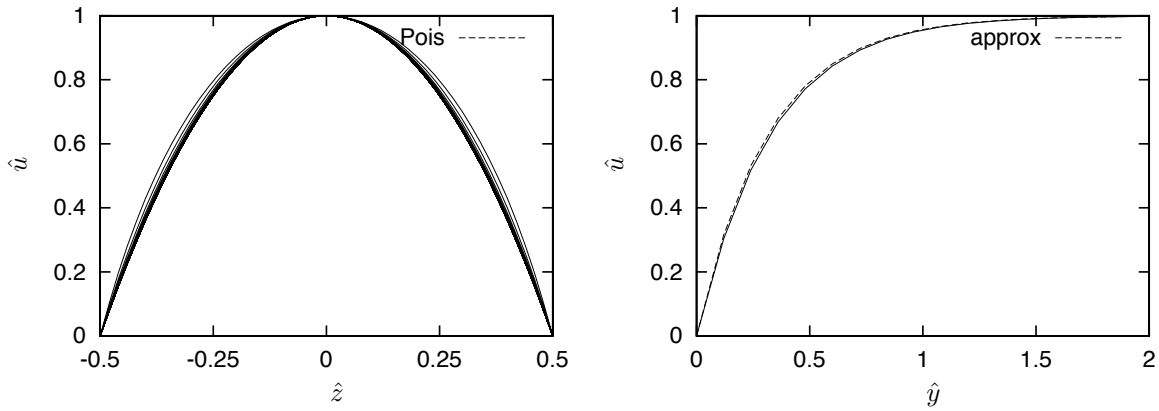

Fig. 2 Basic boundary layer (no bump, $\alpha = 0$) velocity profiles. On the left, the transverse velocity $\hat{u}(\hat{y},\hat{z})/\hat{u}(\hat{y},0)$ (several curves depending on the position $\hat{y}$) is nearly a parabola (dashed curve, "Pois"). On the right, $\hat{u}(\hat{y},0)$ (plain) is compared wih the averaged solution $(1-\exp(-\sqrt{12/\gamma_1}\hat{y}))$, the dashed curve ("approx") corresponds to $(1-\exp(-\sqrt{12}\hat{y}))$, the $\gamma_1 = 6/5$ case with $(1-\exp(-\sqrt{10}\hat{y}))$ is superposed to the computed plain curve.

asymptotic model is of little interest! Next, in making a non-asymptotical approximation, we refine the resolution. We take α smaller than one (but finite) and we use again (13) to compute the slip velocity. This is the so called "weak" coupling with direct resolution of the boundary layer.

We see that the ideal fluid is perturbed by the bump upstream before the bump itself (due to the elliptical behaviour of the Laplacian). The slip velocity is then the velocity at the edge of the boundary layer, and we use it to solve (15), (16), and (14). Using the numerical method presented in the Appendix, we increase the relative size of a given bump (say the very smooth bump $\alpha\bar{f} = \alpha(\exp(-\pi\bar{x}^2))$). This gives the boundary layer displacement $\tilde{\delta}_1$ and the skin friction $\tilde{\tau}$, plotted on figure (3) for various α. For $\alpha = 0.1, 0.2, 0.21, 0.22$, we observe that the deceleration of longitudinal velocity before the bump ($\bar{x} < -1$) induces a small increase of $\tilde{\delta}_1$ and a small decrease in $\tilde{\tau}$. In the wind side of the bump ($-1 < \bar{x} < 0$), the flow is accelerated, the boundary layer is thinner, and there is a large value of the skin friction with a maximum before the crest. In the lee side of the bump, the flow is decelerated, $\tilde{\delta}_1$ becomes larger and larger and $\tilde{\tau}$ approaches 0. For $\alpha = 0.23$, we have incipient separation, which means that there is a point where $\tilde{\tau}$ decreases to zero and then increases. For larger values of α the computation stops at $\tilde{\tau} = 0$. This is the "Goldstein" singularity: when $\tilde{\tau}$ goes to 0, then $\tilde{\delta}_1$ and $d\tilde{\delta}_1/d\bar{x}$ become infinite.

3.2 Triple deck

As was just seen, there is an abrupt change in the boundary layer near the point of zero friction identified by Goldstein (see Cebeci and Cousteix [2] or Gersten and Herwig [7]). To solve the boundary layer separation in the classical boundary layer framework, a "Triple Deck theory" is required (Neiland [17], Stewartson [25], Sychev et al. [26], Smith [23], Sobey [24]). In the Main Deck, we have the inviscid problem:

$$u = \bar{u}_B(\tilde{y}) + \mathrm{Re}^{-1/8}\,\check{A}(\check{x})\,\frac{d\bar{u}_B(\tilde{y})}{d\tilde{y}}\,, \qquad v = -\,\mathrm{Re}^{-1/4}\,\frac{d\check{A}(\check{x})}{d\check{x}}\,\bar{u}_B(\tilde{y})\,, \qquad p = \check{p}(\check{x})\,. \tag{19}$$

The velocity at the edge of the Main Deck is $-\,\mathrm{Re}^{-1/4}\,\frac{d\check{A}(\check{x})}{d\check{x}}$. By asymptotic matching, this is the velocity at the bottom of the Upper Deck, $\check{v}(\check{x},\check{y}=0)$. So the Upper Deck problem now reads :

$$\frac{\partial^2\check{p}_1}{\partial\check{x}^2} + \frac{\partial^2\check{p}_1}{\partial\check{y}^2} = 0\,, \qquad \frac{\partial\check{p}_1(\check{x},0)}{\partial\check{y}} = \frac{d\check{A}(\check{x})}{d\check{x}} + \frac{d^2\check{A}(\check{x})}{d\check{x}^2}\,. \tag{20}$$

In the Upper Deck, we recover the ideal fluid problem (11) at different scales, and with the displacement function $-\check{A}$ instead of the bump shape $\bar{f}$.

In the layer near the wall the contribution of $-\bar{u}$ is in fact negligible, hence we recover the classical Lower Deck equations. These equations are (with $\bar{x} = \mathrm{Re}^{-3/8}\,\check{x}$, $\bar{y} = \mathrm{Re}^{-5/8}\,\check{y}$):

$$\left(\frac{\partial\check{u}}{\partial\check{x}} + \frac{\partial\check{v}}{\partial\check{y}}\right) = 0\,, \tag{21}$$

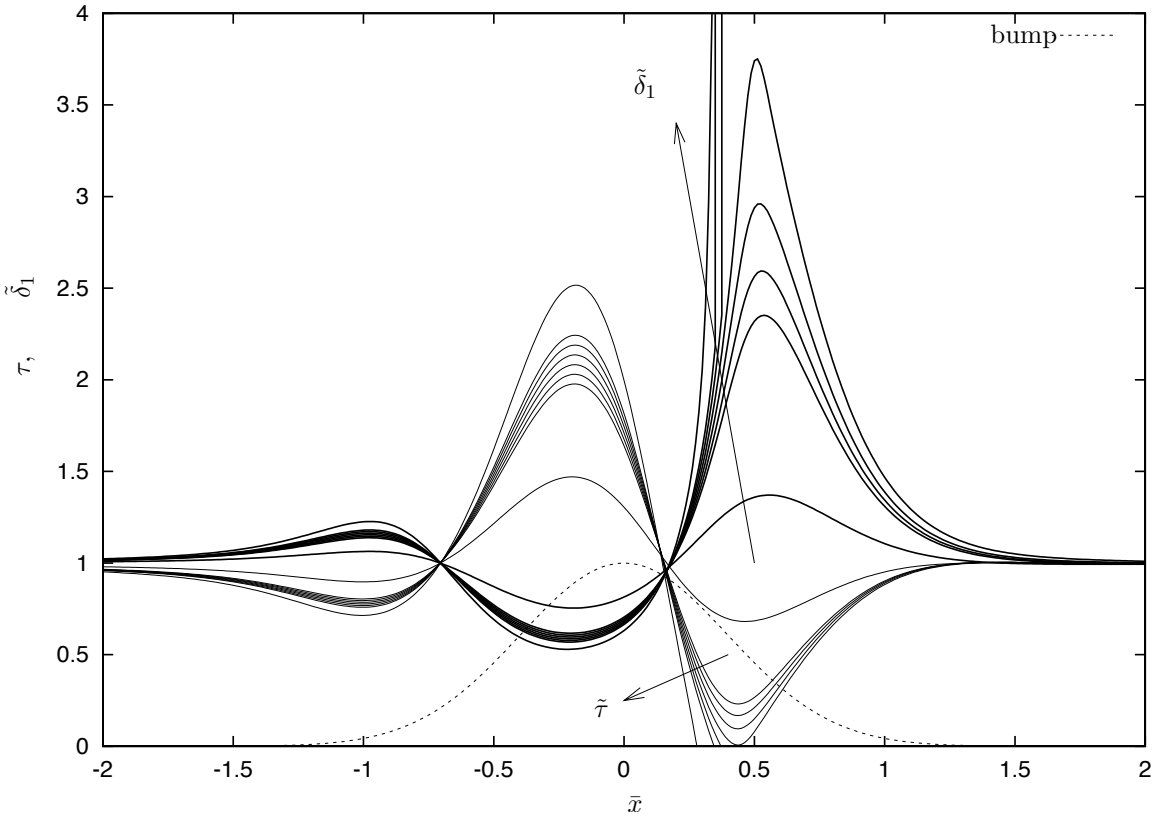

Fig. 3 Case of direct resolution, flow over $\alpha\bar{f} = \alpha e^{-\pi\bar{x}^2}$. Boundary layer displacement $\tilde{\delta}_1$ and skin friction $\tilde{\tau}$ are displayed for various α. The arrows are in the direction of increasing α, for $\alpha = 0.1, 0.2, 0.21, 0.22$ no separation occurs. For $\alpha = 0.23$ we have incipient separation. For $\alpha = 0.24, 0.25, 0.3$ there is a singularity: when $\tilde{\tau}$ goes to 0, $\tilde{\delta}_1$ becomes infinite.

$$\left(\check{u}\frac{\partial\check{u}}{\partial\check{x}} + \check{v}\frac{\partial\check{u}}{\partial\check{y}}\right) = -\frac{\partial\check{p}}{\partial\check{x}} + \frac{\partial^2\check{u}}{\partial\check{y}^2}\,, \tag{22}$$

$$0 = -\frac{\partial\check{p}}{\partial\check{y}}\,, \tag{23}$$

with no slip condition at the wall, no perturbation upstream $\check{u} = \check{y}$, $\check{v} = 0$ and the asymptotic matching of the top of the Lower Deck and the bottom of the Main Deck:

$$\check{u}\,(\check{x}, \check{y} \to \infty) \to \check{y} + \check{A}(\check{x}) \quad \text{and} \quad \check{p}\,(\check{x}, \check{y}) = \check{p}_1\,(\check{x}, 0)\,.$$

An example of comparison is plotted on Fig. 11 right.

3.3 Interactive boundary layer

A simpler way to deal with boundary layer separation is to use the idea of "Interactive Boundary Layer" (Smith [23], Sychev et al. [26], Cebeci and Cousteix [2], Le Balleur [15]). The idea of this theory lies in the fact that, as one reaches separation, $\tilde{\delta}_1$ becomes larger and larger. So, as the Reynolds number is large but finite in practice, the boundary layer will perturbate the ideal fluid. That is to say, displacement thickness becomes of the same size as the size of the bump itself.

This is what happens in the Triple Deck.

Hence, we take into account the perturbation due to the boundary layer in adding to the lower boundary the quantity: $\tilde{\delta}_1\,\mathrm{Re}^{-1/2}$, so that (13) becomes now:

$$\bar{U}_e = 1 + \frac{1}{\pi}\,fp\int_{-\infty}^{\infty} \frac{\frac{d}{d\bar{x}}\left(\alpha\bar{f} + \tilde{\delta}_1\,\mathrm{Re}^{-1/2}\right)}{\bar{x} - \xi}\,d\xi\,. \tag{24}$$

As was said before this term is in fact the next order term. It is not relevant at the considered order. In other words, we consider that the Reynolds is large but finite. So we break the asymptotic sequence of the "weak" coupling. We do a "strong"

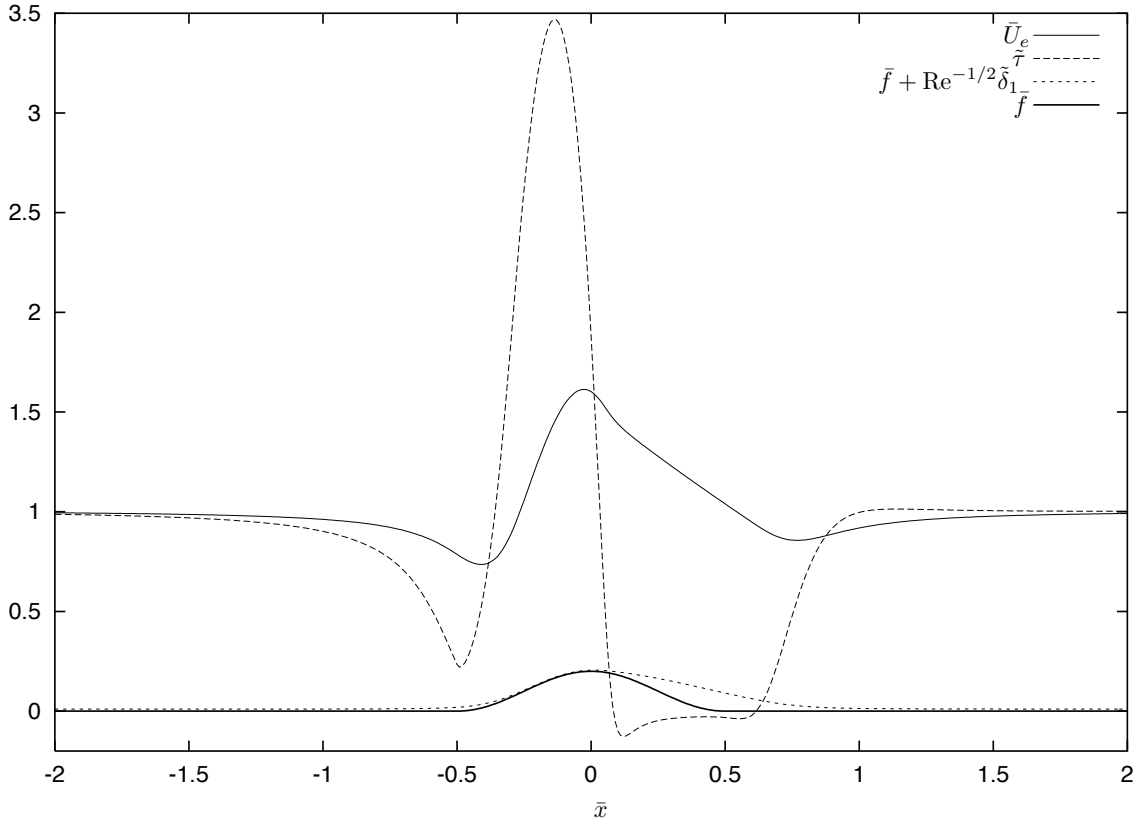

Fig. 4 A typical case of interacting resolution, flow over the arch of sine $\alpha\bar{f} = 0.2(1+\cos(2\pi x))/2$ (for $|x| < 1/2$) at Reynolds Number $\mathrm{Re} = 10^3$. The velocity $\tilde{U}_e$, the skin friction $\tilde{\tau}$, the bump $\alpha\bar{f}$, and the equivalent bump $\alpha\bar{f} + \mathrm{Re}^{-1/2}\,\tilde{\delta}_1$ are plotted.

coupling: the final system is then to solve the strongly coupled set of equations which is the set of boundary layer equations (14)–(16) and the ideal fluid solution (24). They are solved together. One problem of the method was that a small parameter $\mathrm{Re}^{-1/2}$ is still present in the equations.

Dechaume et al. [6] (and Cousteix and Mauss [3] and [4]) established on rational basis the Interactive Boundary Layer equations. They used a "modified van Dyke" principle and "successive complementary expansion method". The existence of a small parameter in the equation is then no more a problem. The link with "Triple Deck" theory is done as well. They show that with this technique the IBL equations are fully justified.

Details of the numerical resolution are given in the Appendix II: the boundary layer must be solved in inverse way, and a coupling semi-inverse procedure is performed.

As an example of resolution we take a given bump which is the arch of sine $\alpha\bar{f} = 0.2(1+\cos(2\pi x))/2$ for $|x| < 1/2$ and zero for $|x| > 1/2$. We show on Fig. 4 typical distributions of the outer edge velocity, the skin friction and the displacement thickness. The interaction result is that the ideal fluid flow "feels" a new bump which is no longer $\alpha\bar{f}$ but $\alpha\bar{f} + \tilde{\delta}_1\,\mathrm{Re}^{-1/2}$. The effect is to smooth the deflection of stream lines after the bump. This deflection may be associated with a separation bulb because the skin friction is negative there.

On Fig. 5 we plot the velocity field ($\tilde{u}, \mathrm{Re}^{-1/2}\,\tilde{v}$, in the Prandtl coordinates) and the displacement thickness (corresponding to a stream line). On the lower part of the figure there is an amplified view of the bump and of the equivalent bump. The perturbation of outer edge velocity is plotted too. It is no longer symmetrical.

Finally on Figs. 6 and 7 we change the parameters Re and α in order to appreciate their influence. On Fig. 6, we increase Re from a non separated configuration to separated ones at fixed α. Increasing the Reynolds number leads to flow separation and to an increase of the maximal shear stress. On Fig. 7, we increase Re at fixed α, this leads to flow separation as well.

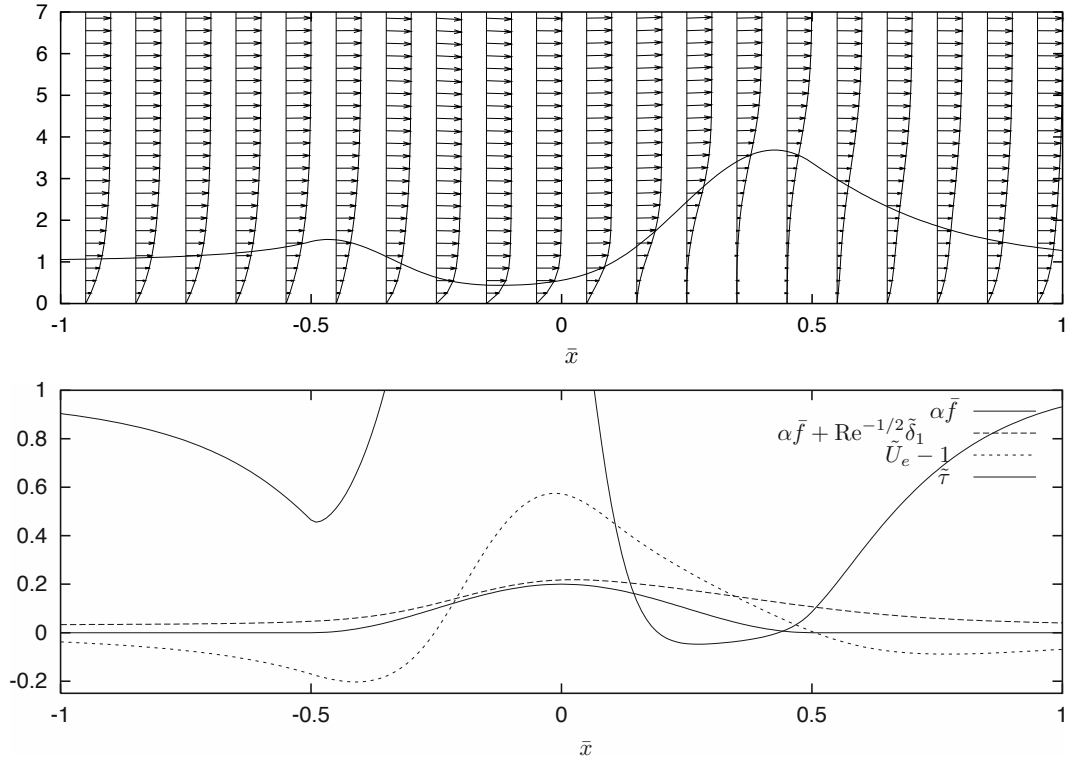

Fig. 5 Interacting resolution, flow over $\alpha\bar{f} = 0.2(1 + \cos(2\pi x))/2$ at Reynolds Number $\mathrm{Re} = 10^3$. Top: velocity profiles ($\tilde{u}/\bar{U}_e$, $\mathrm{Re}^{-1/2}\,\tilde{v}/\bar{U}_e$), and the displacement thickness $\tilde{\delta}_1$ written in Prandtl transformed coordinates. Bottom: The perturbation velocity $(\tilde{U}_e - 1)$, the skin friction $\tilde{\tau}$, the bump $\alpha\bar{f}$, and the equivalent bump $\alpha\bar{f} + \mathrm{Re}^{-1/2}\,\tilde{\delta}_1$ are plotted.

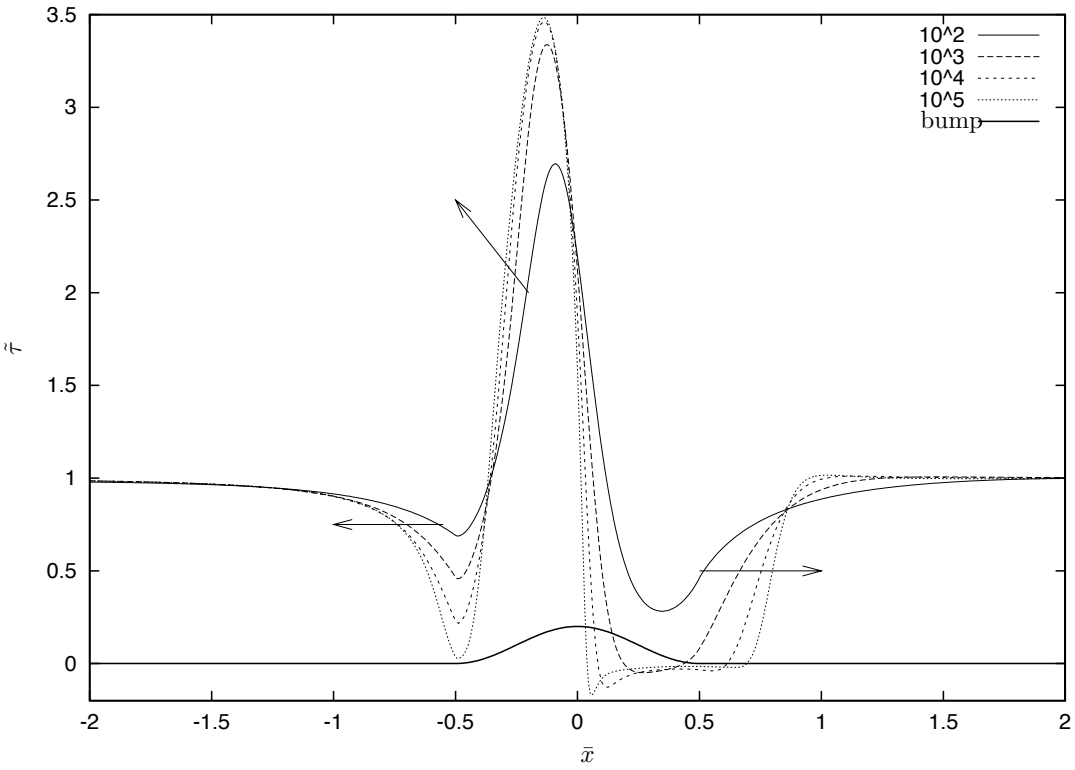

Fig. 6 Case of interacting resolution, flow over $\alpha\bar{f} = 0.2(1 + \cos(2\pi x))/2$. Skin friction as function of $\bar{x}$. Increasing the Reynolds Number Re from 10^2 to 10^5 leads to boundary layer separation in the lee-side (ultimately a secondary recirculation may appear in the stoss-side). The arrows are in the direction of increasing Re.

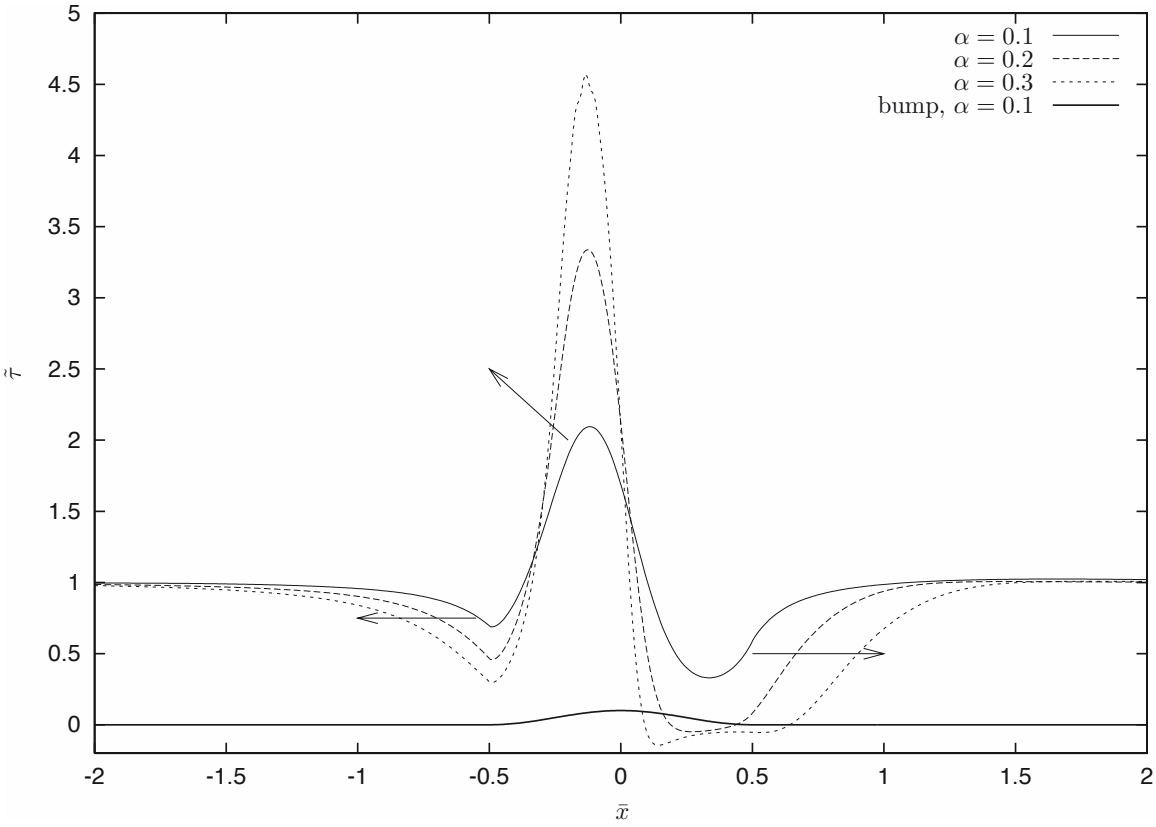

Fig. 7 Case of interacting resolution, flow over $\alpha\bar{f} = \alpha(1+\cos(2\pi x))/2$. Increasing the bump height from $\alpha = 0.1$ to 0.3 at $\mathrm{Re} = 10^3$ leads to boundary layer separation. The arrows are in the direction of increasing α.

4 Comparisons with the full Averaged Navier Stokes equations

The Averaged Navier Stokes system (4)–(6) is solved using the finite element method thanks to FreeFem++ [11]. We wrote the associated variational equation and use the velocity pressure formulation. We solve the problem by the penalty method. P2 elements are used. A 6 x 6 domain is taken, the number of vertices is adjusted by it self and may be of about 9000 vertices. At moderate Reynolds number (10^3) the results are nearly the same for skin friction (Fig. 8). The finite element is very fast and the automatic remeshing allows to put more points in the boundary layer. The computation on a current standard computer system takes about three minutes for FreeFem and less than one minute for the boundary layer code. Those times are only indicative. The computation fails for $\alpha > 0.35$ with the boundary layer code; it takes a very long time to compute this value with FreeFem++.

For larger values of Reynolds number (10^4), the advantage in time of IBL is more obvious (Fig. 9). It takes about one hour for FreeFem and one minute for the boundary layer code. The problem here is that there seems to be no steady solution.

5 Conclusion

Following classical textbooks, a Boundary Layer theory has been settled to solve a special system obtained from Navier Stokes equations averaged along the thin direction. This is only for the Hele Shaw flow. We did not discuss the exact validity of the Averaged Navier Stokes equations, but took them as a starting point. From these equations, we constructed the Averaged Euler equations, and then the Averaged Boundary Layer equation. We showed that the direct resolution leads to a kind of Goldstein singularity. In order to remove this singularity we construct the Interacting Boundary Layer (strong coupling of the ideal and viscous fluid and inverse boundary layer resolution). It means that the boundary layer retroacts on the ideal fluid thanks to the displacement thickness. We adapted boundary layer codes to make the computation. With this point of view, we compute the boundary layer separation which occurs if the bump height is increased, or if the Reynolds number is increased. Furthermore, we favourably compare these computations with a full numerical computation of the Averaged Navier Stokes equations. The boundary layer approach is far quicker.

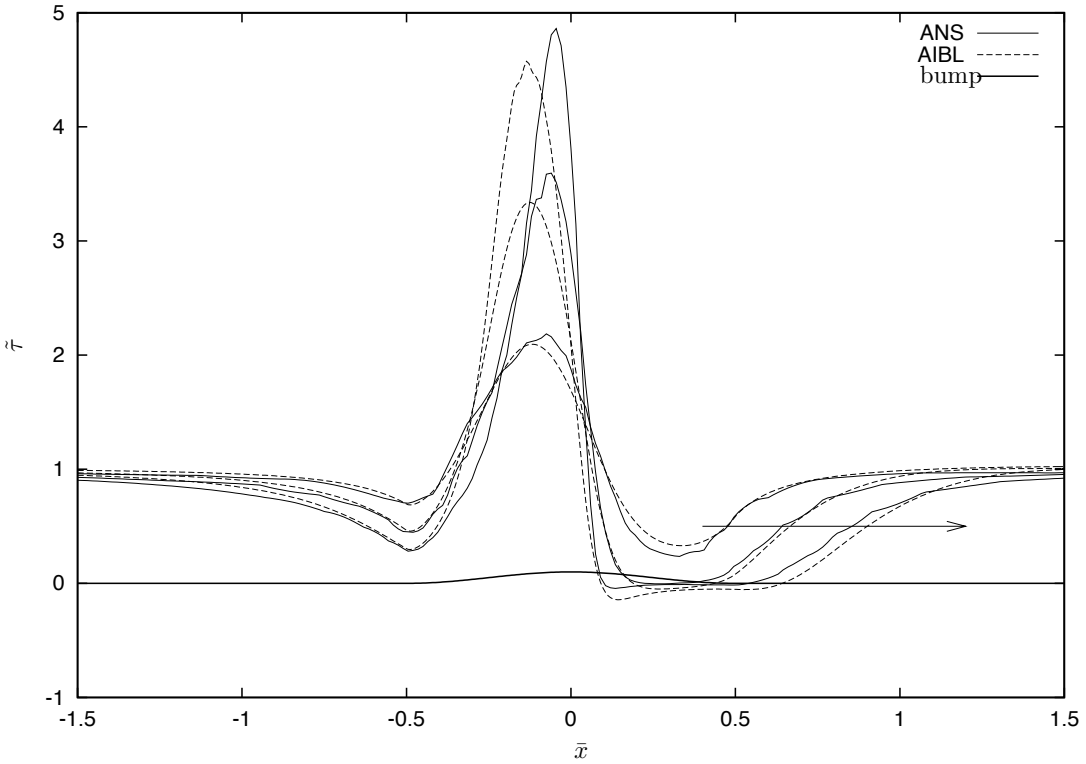

Fig. 8 Wall shear stress. Comparing the Averaged Navier Stokes equations ("ANS", plain line) and the finite differences scheme Keller Box ("AIBL", dashed line) at $\mathrm{Re} = 10^3$ and for three values $\alpha = 0.1$, 0.2, and 0.3 (arrow in the increasing direction). The bump is drawn for $\alpha = 0.1$.

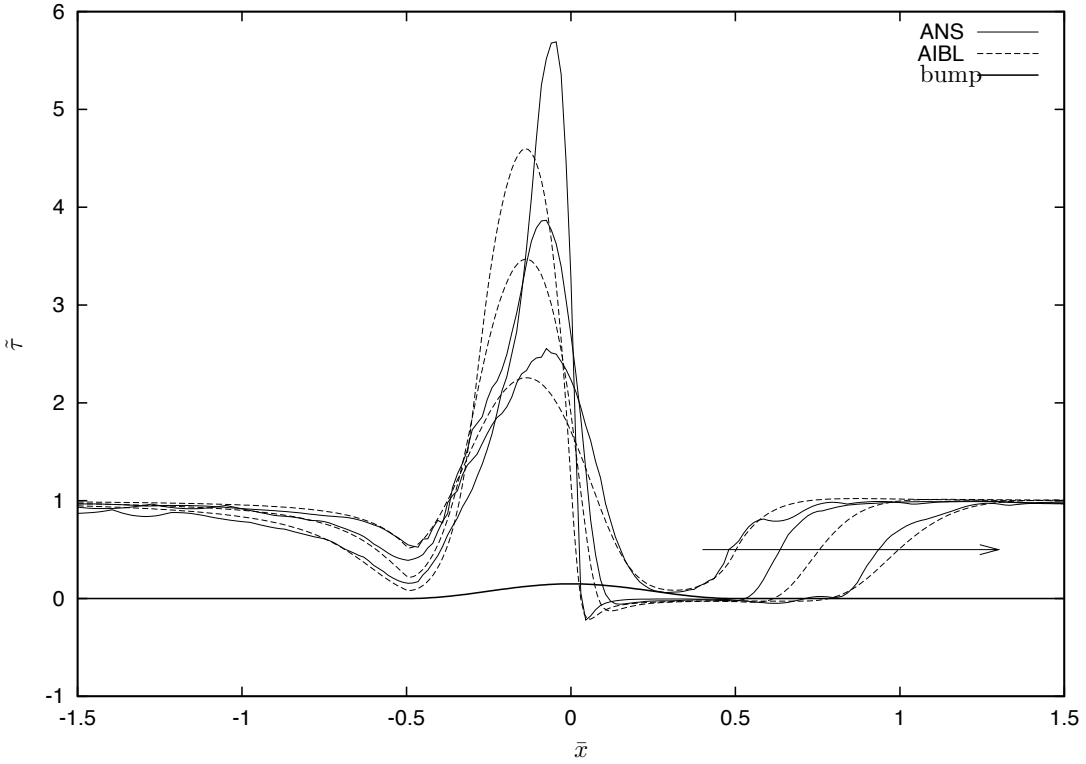

Fig. 9 Wall shear stress. Comparing the Averaged Navier Stokes equations ("ANS", plain line) and the finite differences scheme Keller Box ("AIBL", dashed line) at $\mathrm{Re} = 10^4$ and for three values $\alpha = 0.1$, 0.2, and 0.3 (arrow in the increasing direction). The bump is drawn for $\alpha = 0.1$.

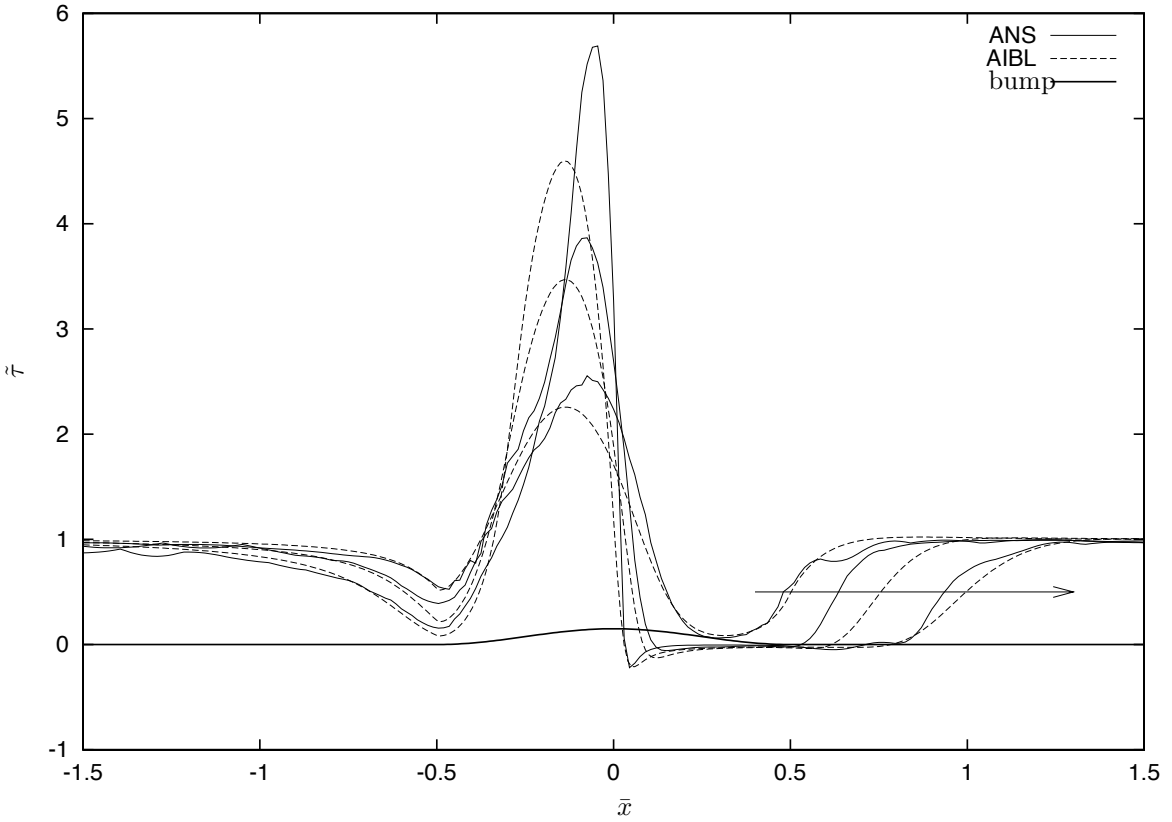

Fig. 10 Pressure along the wall. Comparing the Averaged Navier Stokes equations ("ANS", plain line) and the finite differences scheme Keller Box ("AIBL", dashed line) at $\mathrm{Re} = 10^4$ and for three values $\alpha = 0.1$, 0.2, and 0.3 (arrow in the increasing direction). The bump is drawn for $\alpha = 0.1$.

Of course, all the quantities we computed are averaged ones, so that the separation after the bump may be much more complicated. Especially because of large velocity gradients in this region, the Poiseuille approximation is questionable. Nevertheless, it may be a first approximation to test in experimental setups.

6 Appendix I: an integral method

As is usual in boundary layer theory, we construct an Integral Method. Substracting from the momentum equation (15) the value "at infinity" ($\bar{U}_e \frac{d\bar{U}_e}{d\bar{x}} + \bar{U}_e = -\frac{d\bar{p}}{d\bar{x}}$), we obtain:

$$\left(\frac{\partial \left(\tilde{u} \left(\tilde{u} - \bar{U}_e \right) \right)}{\partial \bar{x}} + \frac{\partial (\left(\tilde{u} - \bar{U}_e \right) v)}{\partial \tilde{y}} + \left(\tilde{u} - \bar{U}_e \right) \frac{\partial \bar{U}_e}{\partial \bar{x}} \right) = \frac{\partial^2 \tilde{u}}{\partial \tilde{y}^2} - \left(\tilde{u} - \bar{U}_e \right) . \tag{25}$$

Integrating from 0 to ∞ all over the boundary layer, and using the following classical definitions:

$$\tilde{\delta}_1 = \int_0^\infty \left(1 - \frac{\tilde{u}}{\bar{U}_e} \right) d\tilde{\delta}_2 = \int_0^\infty \left(\frac{\tilde{u}}{\bar{U}_e} \left(1 - \frac{\tilde{u}}{\bar{U}_e} \right) \right) d\tilde{y} \,, \quad H = \frac{\tilde{\delta}_1}{\tilde{\delta}_2} \,, \quad f_1 = \left. \frac{\tilde{\delta}_1}{\bar{U}_e} \frac{\partial \tilde{u}}{\partial \tilde{y}} \right|_0 , \tag{26}$$

we obtain the "Averaged von Kármán" integral system:

$$\left(\bar{U}_e^2 \frac{d}{d\bar{x}} \left(\frac{\tilde{\delta}_1}{H} \right) + \left(\tilde{\delta}_1 + \frac{2\tilde{\delta}_1}{H} \right) \bar{U}_e \frac{d\bar{U}_e}{d\bar{x}} \right) = f_1 \frac{\bar{U}_e}{\tilde{\delta}_1} - \tilde{\delta}_1 \bar{U}_e \,. \tag{27}$$

It may be solved together with the coupling relation (24) if H and f_1 are known (from $\tilde{\delta}_1$, $\bar{U}_e$). Taking as closure relation the exponential profile: $u_B = 1 - \exp(-\tilde{y})$, we have $H = 2$, $f_1 = 1$, so we may say that we look at perturbations around

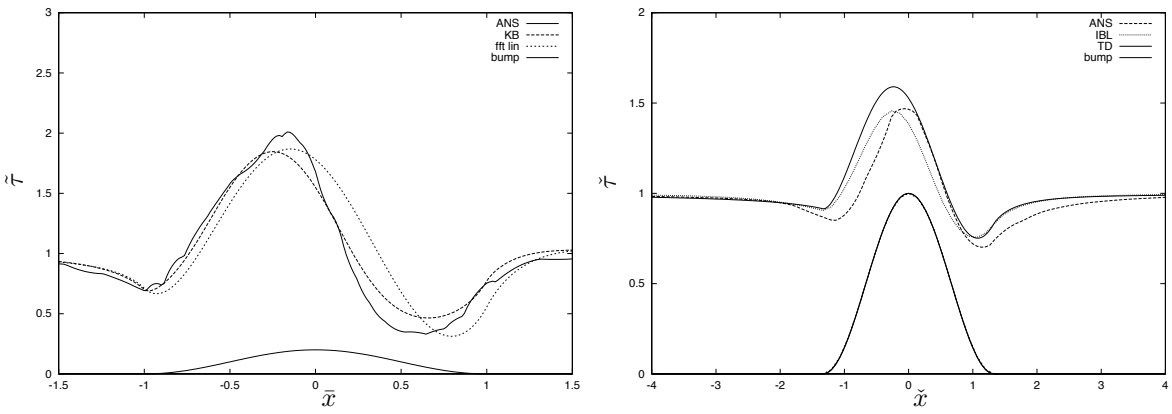

Fig. 11 Wall shear stress. Left: comparing the Averaged Navier Stokes equations ("ANS") and the Keller Box ("KB") and the full linearized solution ("fft lin") at $\mathrm{Re} = 10^3$ and $\alpha\bar{f} = 0.2(1+\cos(\pi x))/2$. Right: comparing the Averaged Navier Stokes equations ("ANS"), Averaged IBL, and Triple Deck ("TD") in triple deck scales at $\mathrm{Re} = 10^3$ on a shorter bump $\alpha\bar{f} = 0.01(1+\cos(2\pi x/0.2))/2$.

the basic state. This will give us a functional relation between $(\bar{U}_e - 1)$ and $(\tilde{\delta}_1 - 1)$. Working in Fourier space and taking the perturbation of (24), we may find the relation between the perturbations and finally, the Fourier transform of the skin friction (with $B(k) = -\frac{2(-ik)}{\frac{(-ik)}{2}+2}$ ratio of $FT[(\tilde{\delta}_1 - 1)]$ by $FT[(\bar{U}_e - 1)]$):

$$(\tilde{\tau} - 1) = FT^{-1}\left[\left(1 - \frac{B(k)|k|\left(1 - |k|\,\mathrm{Re}^{-1/2}\right)}{1 - B(k)|k|\,\mathrm{Re}^{-1/2}}\right)|k|FT\left[\alpha\bar{f}\right]\right]. \tag{28}$$

An example of comparison of this simple formula and the full nonlinear numerical resolution of the problem is displayed on Fig. 11, the over all distribution is not so bad for a so simplified theory up to $\alpha = 0.1$. To improve this we may settle a Pohlhausen method to have better values of H and f_1.

7 Appendix II: semi inverse coupling

Numerical resolution of boundary layer equations is done with an adaptation of the Keller Box ([13] and [2]). It is in inverse way. It means that we give the displacement thickness δ_1 and search the associated edge velocity U_e.

A semi inverse coupling (Le Balleur [15]) is then done. It is an iterative resolution: for a same $\tilde{\delta_1}^n$ distribution two velocities are computed, one $\bar{U}_e^{BL}(\tilde{\delta_1}^n)$ from the boundary layer (15–14), the other one $\bar{U}_e^{IF}(\tilde{\delta}_1^n)$ from the ideal fluid solution (24). The new distribution of displacement thickness $\tilde{\delta_1}^{n+1}$ is then computed by relaxation:

$$\tilde{\delta}_1^{n+1} = \tilde{\delta}_1^n + \mu\left(\bar{U}_e^{BL} - \bar{U}_e^{IF}\right).$$

The iteration is done until convergence. The relaxation parameter μ is chosen to ensure stability of the process (see Le Balleur [15] for details), for example $\mu = 0.5$ for $\mathrm{Re} = 10^3$ but $\mu = 0.25$ for $\mathrm{Re} = 10^4$. For small values of α the two finite differences schemes give the same skin friction, but for increasing values, there is a small difference in the extremal values of $\tilde{\tau}$. Nevertheless, the final $\tilde{\delta}_1$ are superposed. The Fourier resolution of Eq. 28 is done with standard FFT algorithms (Press et al. [20], and Ooura [18]).

References

[1] G. K. Batchelor, An Introduction to Fluid Dynamics (Cambridge University Press, Cambridge, 2000), 608 pp.
[2] T. Cebeci and J. Cousteix, Modeling and Computation of Boundary Layer Flows (Springer Verlag, Berlin, Heidelberg, New York, 1999).
[3] J. Cousteix and J. Mauss, Approximations of the Navier-Stokes equations for high Reynolds number flows past a solid wall J. Comput. Appl. Math. **166**(1), 101–122 (2004).
[4] J. Cousteix and J. Mauss, Analyse Asymptotique et Couche Limite, Mathématiques et Applications, Vol. 56, XII (Springer, Berlin, 2006), 396 pp.

[5] J. S. Darrozès, The method of matched asymptotic expansions applied to problems involving two singular perturbation parameters, Fluid Dyn. Trans. **6**, 119–129 (1971).
[6] A. Dechaume, J. Cousteix, and J. Mauss, An interactive boundary layer model compared to the triple deck theory, Eur. J. Mech. B, Fluids **24**(4), 439–447 (2005).
[7] K. Gersten and H. Herwig, Strömungsmechanik: Grundlagen der Impuls-, Wärme- und Stoffübertragung aus asymptotischer Sicht (Vieweg, Wiesbaden, 1992).
[8] P. Gondret and M. Rabaud, Shear instability of two-fluid parallel flow in a Hele-Shaw cell, Phys. Fluids **9**, 3267–3274 (1997).
[9] P. Gondret, P. Ern, L. Meignin, and M. Rabaud, Experimental evidence of a non-linear transition from convective to absolute instability, Phys. Rev. Lett. **82**, 1442–1445 (1999).
[10] P. Gondret, Rakotomalala, M. Rabaud, D. Salin, and P. Watzky, Viscous parallel flows in finite aspect ratio Hele-Shaw cell: Analytical and numerical results, Phys. Fluids **9**(6), 1841–1843 (1997).
[11] F. Hecht, O. Pironneau, A. Le Hyaric, and K. Ohtsuka, FreeFem++, http://www.freefem.org.
[12] E. J. Hinch and F. Plouraboué, Kelvin–Helmholtz instability in a Hele–Shaw cell: Large effect from the small region near the meniscus, Phys. Fluids **5**, 052107.1–052107.13 (2005).
[13] H. B. Keller, Numerical methods in Boundary Layer theory, Ann. Rev. Fluid Mech. **10**, 417–433 (1978).
[14] P.-Y. Lagrée and S. Lorthois, The RNS/Prandtl equations and their link with other asymptotic descriptions. Application to the computation of the maximum value of the Wall Shear Stress in a pipe, Int. J. Eng. Sci. **43**(3–4), 352–378 (2005).
[15] J. C. Le Balleur, Couplage visqueux non-visqueux: Méthode numérique et applications aux écoulements bidimensionnels transsoniques et supersoniques, Rech. Aerosp. (France) **2**, 67–76 (1978), Eng. Trans ESA TT-496.
[16] T. Loiseleux, P. Gondret, M. Rabaud, and D. Doppler, Onset of erosion and avalanche for an inclined granular bed submitted to a continuous laminar flow, Phys. Fluids **17**, 103304 (2005).
[17] V. Ya. Neiland, Propagation of perturbation upstream with interaction between a hypersonic flow and a boundary layer, Mekh. Zhidk. Gaza (Russia) **4**, 53–57 (1969).
[18] Takuya Ooura, http://momonga.t.u-tokyo.ac.jp/~ooura/ (1997, 2001).
[19] F. Plouraboué and E. J. Hinch, Kelvin-helmholtz instability in Hele-Shaw cell, Phys. Fluids **14**(3), 922–929 (2002).
[20] W. H. Press, B. P. Flannery, S. A. Teukolsky, and W. T. Vetterling, Numerical Recipes in C: The Art of Scientific Computing (Cambridge University Press, Cambridge, 2002).
[21] C. Ruyer-Quil, Inertial corrections to the Darcy law in a Hele-Shaw cell, CRAS **329**(II), 337–342 (2001).
[22] H. Schlichting, Boundary Layer Theory, 7th ed. (McGraw Hill, New York, 1987).
[23] F. T. Smith, Steady and unsteady boundary layer separation, Ann. Rev. Fluid Mech. **18**, 197–220 (1986).
[24] I. J. Sobey Introduction to Interactive Boundary Layer theory, Oxford Applied and Engineering Mathematics (Oxford University Press, Oxford 2000), 256 pp.
[25] K. Stewartson, Multistructured boundary layer on flat plates and related bodies Adv. Appl. Mech. **14**, 145–239 (1974).
[26] V. V. Sychev, A. I. Ruban, V. V. Sychev, and G. L. Korolev, Asymptotic Theory of Separated Flows (Cambridge University Press, Cambridge, 1998).
[27] M. van Dyke, Perturbation Methods in Fluid Mechanics (Parabolic Press, Stanford, CA, 1975).